ELSEVIER

Journal of Structural Geology 29 (2007) 1522–1537

JOURNAL OF STRUCTURAL GEOLOGY

www.elsevier.com/locate/jsg

Strain gradients in zones of ductile thrusting: Insights from the External Hellenides

P. Xypolias*, V. Chatzaras, I.K. Koukouvelas

Department of Geology, University of Patras, GR-26500 Patras, Greece

Received 14 December 2006; received in revised form 29 April 2007; accepted 29 May 2007
Available online 27 June 2007

Abstract

New finite strain data from a thrust-sense shear zone, which extends for 600 km along-strike in the high-pressure belt of the External Hellenides (Greece), were used to describe the variation of ductile strain with structural distance (D) from the basal thrust. Sampling was carried out along four traverses across the central and southeastern parts of the zone. The strain ratio in XZ sections (R_{XZ}) of 120 samples was obtained using the theta-curve, the mean object ellipse and the mean radial length methods. All methods give very consistent results. Based on these results, four strain profiles were constructed depicting a non-linear increase of R_{XZ} values with proximity to the basal thrust. These profiles in combination with published strain data from the northwestern parts of the zone enabled us to obtain an empirical logarithmic function describing the relationship between R_{XZ} and D. This function includes only one varying parameter, which represents the strain gradient in linear $R_{XZ} - \ln D$ space. The value of strain gradient is directly correlated with the strain level in the thrust zone and provides information for strain localization at its base. The proposed function may also be used for quantifying the strain profiles of ductile to semi-ductile thrust zones in other orogenic belts such as the Alps, the Appalachians and Himalaya.

Keywords: Strain; Ductile thrust; High-pressure shear zone; Phyllite–Quartzite unit; Greece

1. Introduction

Ductile shear zones ranging in thickness from millimetres to kilometres are common deformational features of collisional belts (e.g. Burg, 1999; Carreras, 2001). It is widely accepted that they control strain localization on various scales in the continental crust during mountain building. For a typical continuous shear zone (Ramsay and Graham, 1970; Ramsay, 1980) with monoclinic symmetry (Passchier, 1998), the strain profile (XZ) parallel to the shear direction (X) and normal to the shear zone plane (XY), shows a non-linear increase of strain from the shear zone margins towards its centre (e.g. Burg and Laurent, 1978; Ramsay and Huber, 1983; Sørensen, 1983; Fusseis et al., 2006). However, some strain studies of outcrop scale shear zones emphasize that both finite strain and shear strain are often localized into discrete bands parallel to the plane of the shear zone (Dutruge et al., 1995; Arbaret and Burg, 2003). Even so, the overall pattern of strain variation with distance from the shear zone centre could be described by a smoothed non-linear curve, which often obeys an exponential function (Dutruge and Burg, 1997).

On a crustal scale, several strain profiles from ductile to semi-ductile thrust zones also display analogous patterns implying a non-linear increase of X/Z strain ratios (R_{XZ}) towards a basal thrust (Mitra, 1979; Ramsay, 1981; Sanderson, 1982; Williams et al., 1984; Merle, 1989; Gray and Willman, 1991; Dittmar et al., 1994; Grasemann et al., 1999; Xypolias and Kokkalas, 2006). This strain increase is often documented by an observed strain zonation in the thrust hanging-wall defined by three thrust-parallel sub-zones, each of which records a roughly homogeneous finite strain (Gray and Willman, 1991; Yassaghi et al., 2000; Yonkee, 2005). In such cases, the thickness of the lowermost sub-zone which records the higher strain

* Corresponding author. Tel./fax: +30 2610 994485.
E-mail address: p.xypolias@upatras.gr (P. Xypolias).

0191-8141/$ - see front matter © 2007 Elsevier Ltd. All rights reserved.
doi:10.1016/j.jsg.2007.05.006

values is generally considerably smaller than those of the bordering sub-zones. Moreover, the relative thickness and the strain level of homologous sub-zones belonging to different thrust sheets could be disparate. Apart from the competence of the rocks in a deforming thrust sheet, strain gradients are also strongly dependent on the deformation temperature and the crustal depth (Dittmar et al., 1994; Butler et al., 2002). Relatively low and extremely localized strain close to the basal thrust is commonly recorded at upper crustal levels, while greater and more widely distributed strain can be observed at progressively deeper crustal levels (Yonkee, 2005 and references therein). This implies that the analysis of strain gradients is an essential prerequisite in understanding how rocks deform (Horsman and Tikoff, 2007) in zones of ductile thrusting.

This paper presents new strain data and describes finite strain profiles from several locations across a thrust-related shear zone which extends for roughly 600 km along-strike within the high-pressure (HP) belt of the External Hellenides. It will be shown that strain variation with distance from the basal thrust can be described by a simple logarithmic function with only one varying parameter. The proposed function appears to describe satisfactorily the strain patterns in other naturally occurring thrust-related shear zones and thrust sheets in the Helvetic Alps, the central Appalachians, the eastern Nepal Himalaya and the Klamath Mountains.

2. Geological framework

The HP-belt of the External Hellenides is made up of the Phyllite–Quartzite (PQ) and the Plattenkalk rock units cropping out in the cores of several windows in the Peloponnese and the islands of Kythira and Crete (Fig. 1; e.g. Seidel et al., 1982). It extends along strike over 600 km and in map-view is characterized by a pronounced convex-to-the-foreland

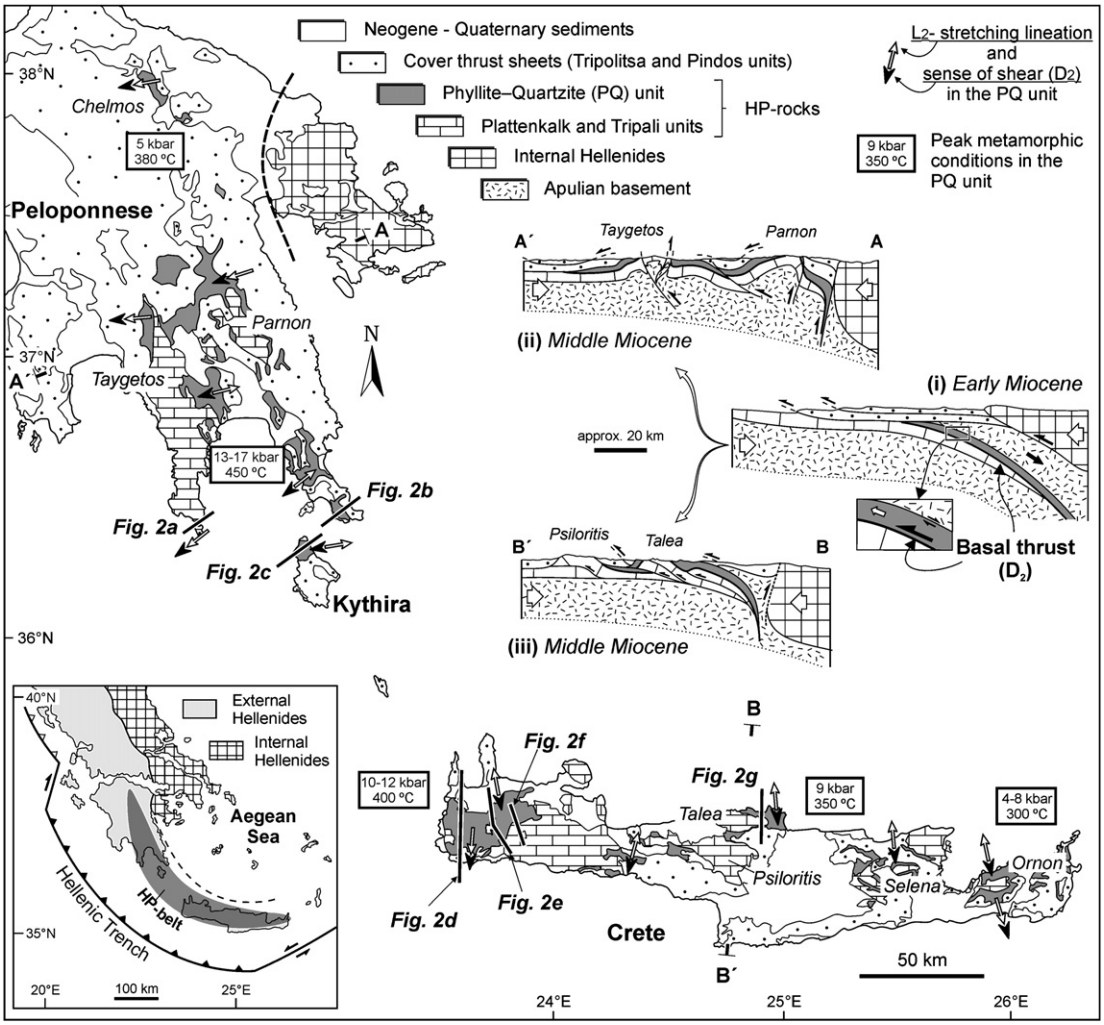

Fig. 1. Simplified geological map of the southwest External Hellenides. L_2 stretching lineation, sense of shear (D_2) and peak metamorphic conditions in the PQ unit are also shown. Structural data after Baumann et al., 1976; Greiling, 1982; Doutsos et al., 2000; Xypolias and Koukouvelas, 2001; Zulauf et al., 2002; Kokkalas and Doutsos, 2004; Chatzaras et al., 2006. Metamorphic data after Katagas et al., 1991; Theye et al., 1992; Blumör, 1998. Evolutionary profiles (i), (ii) and (iii) denote two main events of the orogenic evolution of the External Hellenides in Peloponnese (AA′; e.g. Xypolias and Doutsos, 2000; Doutsos et al., 2006) and Crete (BB′; e.g. Chatzaras et al., 2006). During ductile D_2-event (i) the PQ unit was extruded upward and emplaced onto the Plattenkalk unit via the basal thrust. The geographic location of transects in Fig. 2 are also shown. Inset shows the HP-belt of the External Hellenides and the active Hellenic Arc.

parabolic curvature that can be followed along the active Hellenic Arc (Fig. 1, inset). The PQ unit constitutes the body of the studied shear zone. It is considered to be a metamorphosed Late Carboniferous–Upper Triassic rift sequence consisting of phyllites, quartzites, metaconglomerates and marble intercalations (Robertson, 2006 and references therein). The thickness of the PQ unit is ca. 2 km in the central parts of the shear zone (Kythira, westernmost Crete; Fig. 1) and decreases systematically towards its lateral tips (north Peloponnese, east Crete; Fig. 1) where it approaches ca. 1 km. The PQ unit is tectonically emplaced on the Plattenkalk unit by a major ductile thrust (Baumann et al., 1976; Greiling, 1982; Avigad et al., 1997; Doutsos et al., 2000; Zulauf et al., 2002; Ring and Reischmann, 2002), the "basal thrust" (Figs. 1, 2). The structurally lower Plattenkalk unit is composed of Carboniferous–Eocene carbonate rocks overlain by an Oligocene limy metaflysch with metaconglomerate horizons (e.g. Kowalczyk et al., 1977). Exceptionally in west Crete, an Upper Triassic–Lower Jurassic carbonate sequence, the Tripali unit, lies tectonically between the Plattenkalk and the PQ units (Fig. 2d–f). The PQ unit is, in turn, overlain by the Tripolitsa and Pindos units representing the cover thrust sheets (Figs. 1, 2). They are mainly composed of Mesozoic carbonate rocks and show evidence of very low-grade metamorphism at their base (Tripolitsa unit; e.g. Feldhoff et al., 1991). Relic slices of the pre-Alpine basement orthogneiss occasionally occur along the tectonic contact between the PQ and the Tripolitsa units (Fig. 2c; Xypolias et al., 2006).

In Oligocene times the PQ unit protolith underthrust beneath the Tripolitsa unit basement (e.g. Xypolias and Doutsos, 2000; Doutsos et al., 2000), resulting in HP-metamorphism, dated at ca. 24 Ma (Seidel et al., 1982). Peak metamorphic conditions in the PQ unit (Fig. 1) decrease systematically in

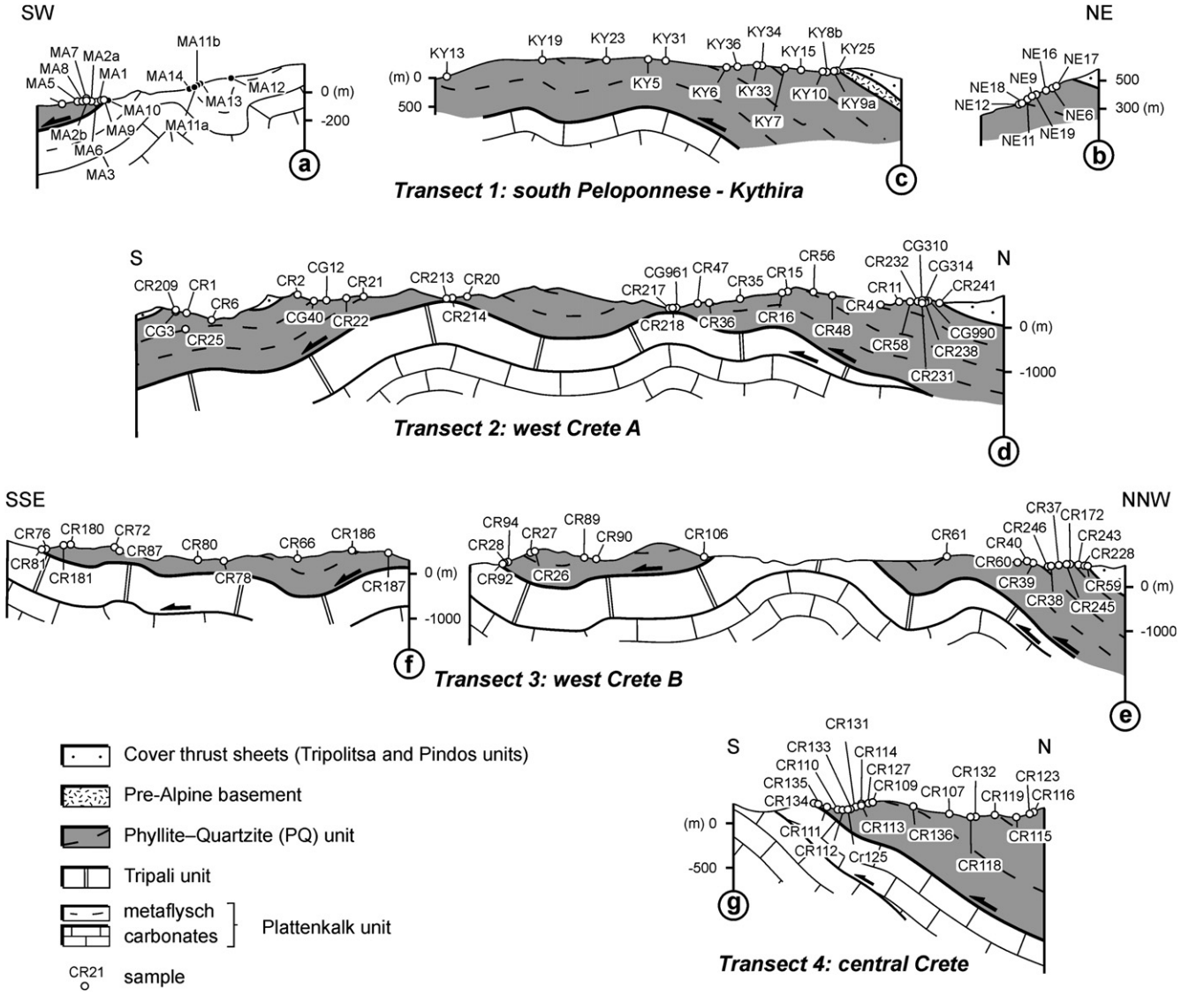

Fig. 2. Cross-sections illustrating the structural position of the samples in the shear zone; locations of sections are shown in Fig. 1. Note that the flexural geometry of the zone was formed during the late-stage (semi-brittle) exhumation, which followed the ductile extrusion and emplacement of the PQ onto Plattenkalk unit.

map-view from the central parts to the lateral tips of the shear zone (e.g. Theye et al., 1992). Subsequent near-isothermal decompression and exhumation of the PQ unit rocks began in Lower Miocene (Thomson et al., 1998), when they detached from their basement and extruded upwards between the basal thrust and the Tripolitsa unit basement at the top (Fig. 1 (i); Doutsos et al., 2000; Xypolias and Doutsos, 2000). Strain and kinematic vorticity studies in central and north Peloponnese indicate that ductile deformation during west-directed extrusion of the PQ unit was characterized by a non-linear down-section increase of both total finite strain and simple shear component, under conditions that generally do not deviate significantly from plane-strain (Xypolias and Koukouvelas, 2001; Xypolias and Kokkalas, 2006). Plane-strain deformation is also prominent in the PQ unit rocks of east Crete (Zulauf et al., 2002; Kokkalas and Doutsos, 2004). The end effect of this extrusion process was the emplacement of the PQ unit on the Plattenkalk unit and its juxtaposition with the overlying cover thrust sheets along an "apparent" normal fault. Regional out-of-sequence thrusting, backthrusting and folding of the shear zone under semi-brittle conditions took place in Middle Miocene (Fig. 1 (ii), (iii); Chatzaras et al., 2006; Doutsos et al., 2006; Kokkalas et al., 2006). These late-stage structures were responsible for the flexural geometry of the shear zone seen in cross-section (Fig. 2).

3. Major fabric elements and deformation mechanisms in the shear zone

The PQ unit has experienced at least two events of ductile deformation (D_1, D_2). The earlier D_1 structures are poorly preserved in the form of minor isoclinal folds (Zulauf et al., 2002) and as a relic internal foliation (S_1) in porphyroclastic HP-related minerals (e.g. glaucophane, chloritoid; Seidel et al., 1982). D_2-related fabrics are by far the most common structural elements in the PQ unit and are genetically related to the extrusion process in Lower Miocene times (e.g. Doutsos et al., 2000). D_2 produced a penetrative foliation (S_2) sub-parallel to the basal thrust that post-dates the main growth of the HP-minerals (Theye et al., 1992; Xypolias and Kokkalas, 2006). Well-developed within the plane of S_2 is a mineral-stretching and clast-elongation lineation (L_2) trending perpendicular to the structural grain of the shear zone (Fig. 1). The maximum asymmetry of several kinematic indicators is observed on sections parallel to L_2 and perpendicular to S_2 (*XZ*—principal plane of finite strain) indicating monoclinic ductile deformation during D_2 (e.g. Xypolias and Koukouvelas, 2001). Throughout the shear zone, kinematic indicators confirm consistent foreland-directed transport (Fig. 1).

Quartzites of the PQ unit show evidence of extensive dynamic recrystallization accommodated by both subgrain rotation and low-temperature grain-boundary migration (regime 2 of Hirth and Tullis, 1992). This, in addition to the presence of strong quartz c-axes preferred orientation patterns suggest that dislocation creep was the dominant deformation mechanism during D_2 shearing (Xypolias and Kokkalas, 2006 and references therein). Evidence for deformation by dissolution precipitation creep is mainly restricted to metasiltstones, where quartz clasts are embedded in a phyllosilicate-rich matrix and occasionally show pressure shadows on both sides of grains (Schwarz and Stöckhert, 1996).

4. Finite-strain analysis

This study presents new finite-strain data from the central (south Peloponnese) to eastern (central Crete) parts of the shear zone occupying in plan-view a 300 km long segment within it (Fig. 1). Previous finite-strain studies have been focused on areas covering the lateral terminations of the zone (Fig. 1; Chelmos, Taygetos–Parnon, Selena–Ornon windows; Xypolias and Kokkalas, 2006 and references therein).

4.1. Sampling

A total of 116 oriented samples from different structural levels above the basal thrust were analysed to obtain estimates of the axial ratio of the finite strain in *X*/*Z* sections (R_{XZ}). Six samples located beneath the basal thrust were also analysed. Sampling was carried out in four main transects trending parallel to the shear direction (Fig. 2); the south Peloponnese–Kythira (38 locations), the west Crete A (33 locations), the west Crete B (31 locations) and the central Crete (20 locations) transect. Details of sample locations and estimated sampling distances measured perpendicular to the basal thrust are given in Fig. 2 and Appendix A.

Attempting to describe the overall pattern of finite strain variation, our sampling strategy was to avoid mesoscopic deformation zones with strain localization effects. Moreover, samples were collected from stratigraphically coherent horizons to reduce lithologically induced strain heterogeneities. All analysed samples are characterized by a single, homogeneously developed, penetrative S_2 foliation.

4.2. Strain methods and markers

Finite-strain ratio R_{XZ} was estimated using graphical and algebraic *Rf*-*φ* methods (cf. Lisle, 1994; see below). Elliptical strain markers (Ramsay and Huber, 1983) such as plastically deformed quartz grains and clasts in fine-grained metaconglomerates, metapsammites, metasiltstones and quartzites were analysed in 109 samples. Elliptical pebbles and cobbles in metaconglomerate horizons from 13 road-cut sections were also analysed. The Fry method (Fry, 1979) was also applied to nineteen representative samples to determine matrix strain and to compare it with particle strain observed with *Rf*-*φ* analysis.

It is emphasized that strain analysis was not carried out in pure quartzites showing extensive dynamic recrystallization because the shape of the most deformed grains may have restored to more equant form (Fig. 3a; e.g. Law, 1986). However, analysis was performed in a few quartzites that include slightly recrystallized quartz ribbons embedded in a fine-grained quartzose matrix (Fig. 3b). Generally, the extent of recrystallization in quartz grains appears to decrease drastically as the phyllosilicate (chiefly mica) content increases

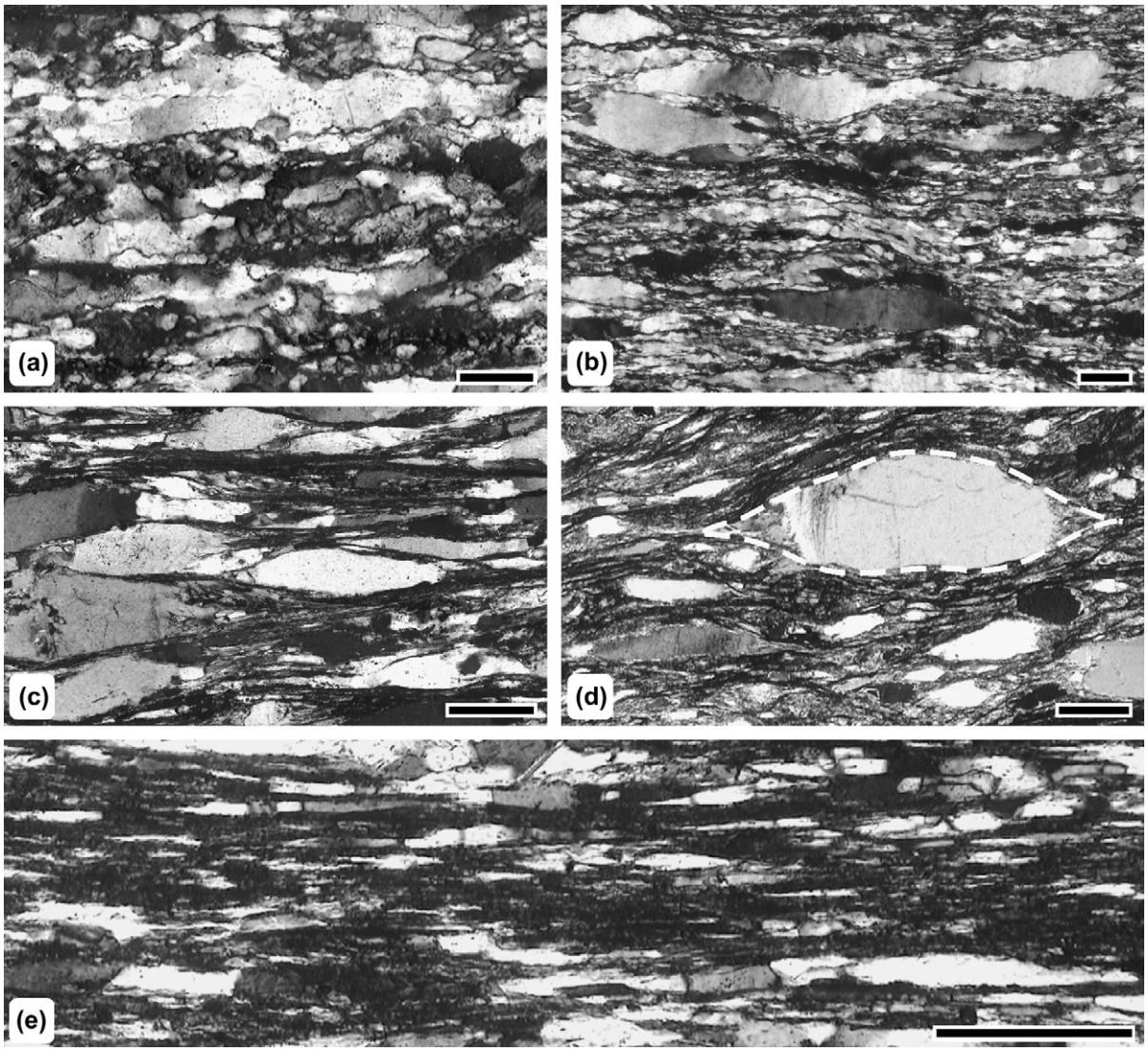

Fig. 3. Micrographs (crossed nicols) of samples from the PQ unit; all micrographs are from thin sections oriented parallel to the L_2-stretching lineation and perpendicular to foliation (*XZ*-plane). Scale bar in each micrograph is 0.2 mm. (a) Sample CR125: pure quartzite showing evidence of extensive dynamic recrystallization. The shape of plastically elongated quartz grains is considered to have been significantly modified by the recrystallization processes. (b) Sample CR133: slightly recrystallized quartz ribbons with undulose extinction are embedded in a fine-grained quartzose matrix. (c) Sample CR20: phyllosilicate aggregates are deflected around plastically deformed quartz grains resulting in an anastomosing fabric. (d) Sample CR27: pressure shadows at both ends of the quartz clast (center) form a smoothly-tapered shape and imply that mass transfer process was active during deformation. (e) Sample MA5: plastically deformed quartz grains embedded in a fine-grained phyllosilicate matrix.

(see Wilson, 1982 for a similar case). The majority of analysed samples are characterized by the presence of mica aggregates that anastomose around plastically elongated quartz grains or clasts (Fig. 3c,e) showing evidence of undulose extinction. Although, strain was mainly accommodated by crystal-plasticity there is evidence showing that mass transfer processes were also active. In such cases, the removed quartz material seems to have been added to both ends of the marker in a smoothly-tapered shape (Fig. 3d). Generally, the effects of mass transfer processes were distributed along grain margins in a way that the *Rf-φ* analysis yielded reliable results (Onasch, 1984).

For each sample, digital photographs of road-cut or thin sections parallel to the *XZ*-plane were taken. In general, the traces of 50–250 (Appendix A) grain outlines were input into the software package SAPE (Mulchrone et al., 2005), which automatically approximates complex grain shapes as ellipses and extracts *Rf-φ* data. Three methods using *Rf-φ* data were applied: the *theta-curve* (Lisle, 1977), the *mean object ellipse* (Erslev and Ge, 1990) and the *mean radial length* (Mulchrone et al., 2003) method. The reason for applying three methods is twofold; to compare their results as well as the strain patterns within the shear zone that they record. In the following, we briefly summarize our application.

The theta-curve (TC) method is based on progressive unstraining of an ellipse data set until a uniform distribution arises and finds a best-fit strain value that minimizes a χ^2 statistic (Lisle, 1977, 1985). Strain calculation was made utilizing the computer-based approaches of Mulchrone and Meere

(2001) and Chew (2003). Following the approach of Yonkee (2005), uncertainties in best-fit R_{XZ} values were evaluated using bootstrap resampling. The resamples of strain values producing χ^2 below a threshold value were generally characterized by normal distribution with standard deviations ≤ 0.3.

The mean object ellipse (MOE) method calculates the best-fit strain ellipse by using a least-square algorithm. It also provides the average radial error of the calculated strain ellipse. MOE routines were executed using the software package INSTRAIN (Erslev and Ge, 1990). The same software was also used for Fry analysis.

The mean radial length (MRL) method is based on the fact that averaging the parameters of an initial ellipse distribution (unstrained state) defines a circle, so that in the strain state the averaged parameters define the strain ellipse. The calculations of the finite strain ratio and the associated analytical error were implemented in a spreadsheet application using the mathematics described in Mulchrone et al. (2003) and Mulchrone (2005; his equations 19, 20, 25), respectively.

4.3. Results

Comparison of R_{XZ} values obtained by the Fry and the *Rf-φ* methods in samples covering the whole range of analysed lithologies revealed small differences. For instance, the scatter graph of Fry versus TC strains shows a very good linear correlation with the slope of the regression line through the origin to be nearly 1 (Fig. 4a). Therefore, we conclude that competence contrast between matrix and clasts was not significant during strain accumulation. Similar conclusion has been drawn by strain studies in the central Peloponnese (Xypolias and Kokkalas, 2006) as well as in east Crete (Zulauf et al., 2002). Hence it seems reasonable that the results of *Rf-φ* analyses are meaningful and reflect bulk strain in the samples. The comparison of the three applied *Rf-φ* methods also reveals a very good consistency between their results. However, the linear-regression analysis implies that the TC method gives slightly higher R_{XZ} values than the MRL (Fig. 4b) and slightly lower than the MOE method (Fig. 4c).

Data from the *Rf-φ* strain analyses (Appendix A) were plotted against distance (D) from the basal thrust to examine the variation of R_{XZ} values along four transects (Fig. 5). As a whole, the resultant profiles show a systematic strain increase with proximity to the basal thrust. However, strain gradient is not constant from the top to the bottom of the shear zone. A slight increase in strain ratio from ca. 3–4 at the uppermost levels (1200–2000 m above the basal thrust) of the zone to ca. 4–6 at a projected distance of 400–600 m above the basal thrust is observed for the profiles in Crete (Fig. 5b,c,d). In south Peloponnese–Kythira, the R_{XZ} values at the top of the zone are higher ranging mostly from 5 to 6.5 (Fig. 5a). The shear zone domain between ca. 500 and ca. 100 m above the basal thrust is characterized by a relatively high strain gradient, corresponding to an increase in R_{XZ} values from ca. 5 to ca. 7 (Fig. 5). Within 100 m of the basal thrust, finite strain ratios increase markedly reaching values of 9 and 14 in Crete (Fig. 5b–d) and south Peloponnese (Fig. 5a), respectively. However, it should be emphasized that higher strain values are expected within the lower 10 m proximal to the basal thrust where mylonitic rocks are observed. For these rocks, strain analysis cannot give reliable results due to strong recrystallization. Moderately high strain ratios of around 6 are recorded below the basal thrust in the south Peloponnese (Fig. 5a).

Summarizing, the aforementioned features of strain profiles are indicative of a progressive non-linear strain increase towards the basal thrust. Few local peaks in strain values (i.e. 1850 m in Fig. 5b; 170 m in Fig. 5d), showing deviation from the bulk trend of the profiles, are interpreted to reflect discrete zones of localized deformation.

5. Correlation function between strain ratio and distance

Results of this work are in agreement with previous studies in the shear zone (e.g. Xypolias and Kokkalas, 2006) also

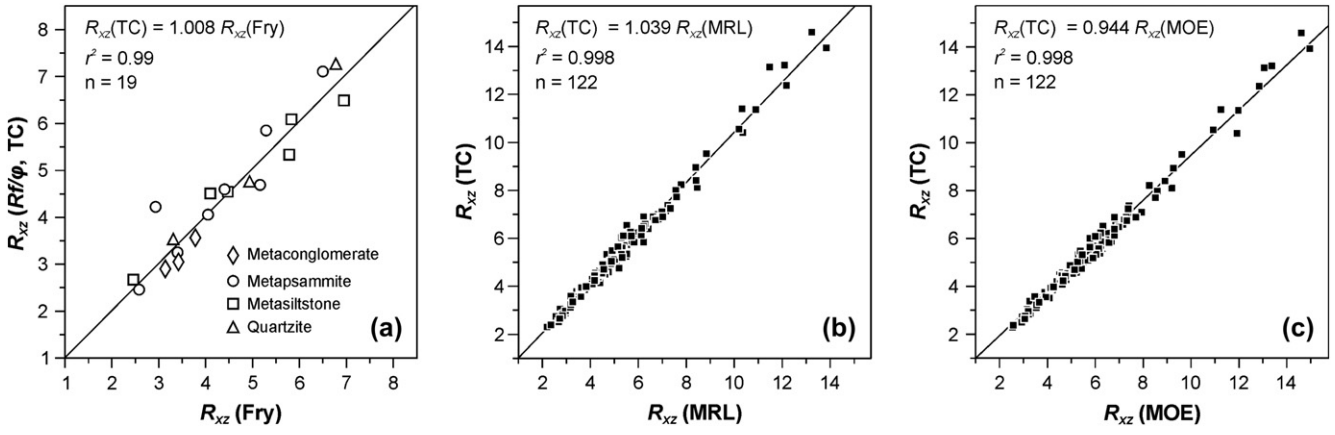

Fig. 4. Plots of R_{XZ} values calculated using TC (R_{XZ}(TC)) method against R_{XZ} values calculated using: (a) Fry (R_{XZ}(Fry)), (b) MRL (R_{XZ}(MRL)) and (c) MOE (R_{XZ}(MOE)) methods. Best-fit straight lines through the origin are shown.

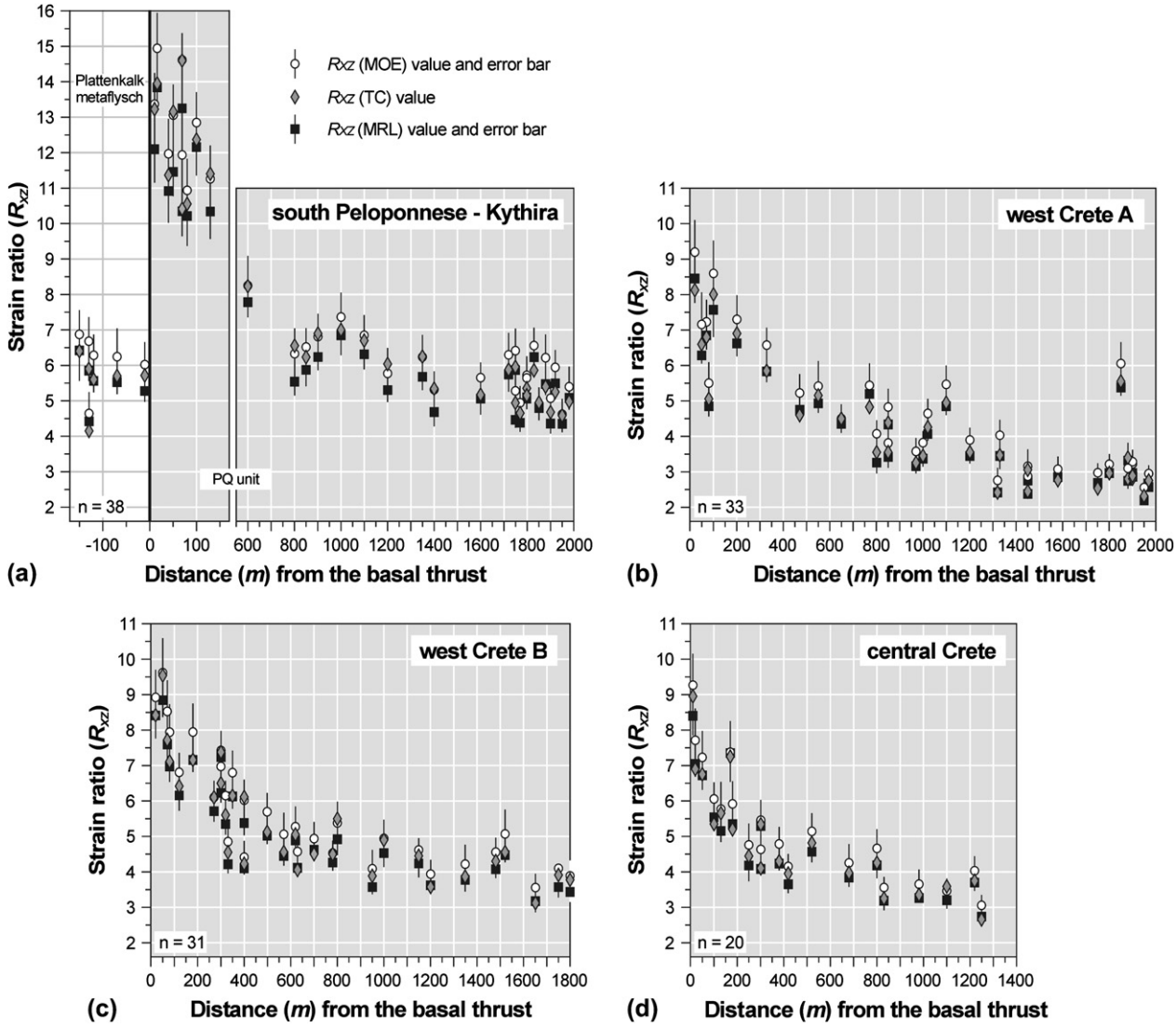

Fig. 5. Graphs illustrating the variation in R_{XZ} (strain ratio in XZ-section) values versus structural distances from the basal thrust along four profiles; error bars are also shown. R_{XZ}(TC), R_{XZ}(MRL), R_{XZ}(MOE): strain ratio obtained by applying the TC, the MRL and the MOE methods, respectively. For location of profiles see Figs. 1, 2. Raw data are listed in Appendix A.

suggesting a non-linear finite strain increase with proximity to the basal thrust. With this observation in mind, we attempt to derive an empirical function describing the relationship between R_{XZ} and D throughout the shear zone. For this purpose, we analysed the four new profiles described above as well as two profiles from the north (Chelmos window; Fig. 1) and central Peloponnese (Taygetos–Parnon window; Fig. 1). Note that strain data from the PQ unit in eastern Crete are not included in the following analysis. In this area, finite strains are complicated by the formation of a number of internal thrust sheets (Zulauf et al., 2002; Robertson, 2006).

5.1. Regression analysis

Following the common practice when non-linear relationships are thought to be present, we sought a procedure that permits their description by the much simpler linear equation. Our search revealed that scatter plots of R_{XZ} versus natural logarithms of D values are characterized by a linear trend of the data points implying a linearizable correlation function of equation type:

$$R_{XZ} = \alpha - \beta \ln D \tag{1}$$

where α and β are the R_{XZ}-axis intercept and the slope of the straight line, respectively. The results of least-squares regression analysis attempting to fit the Eq. (1) to the R_{XZ} and D data sets are summarized in Table 1. Statistical test of the linear association between R_{XZ} and $\ln D$ showed that the observed coefficient of correlation (r, Table 1) is significant at 0.001 probability level of testing and therefore, the null hypothesis (zero correlation) is rejected. Analysis of variance was also performed in order to test the statistical significance of the

Table 1
Results of regression analysis

Profile	n	$R_{XZ} = \alpha - \beta \ln D$					$R_{XZ} = \beta(10.25 - \ln D)$	
		r^2	r	$\alpha \pm$ SE	$\beta \pm$ SE	F/p (ANOVA)	r^2	$\beta \pm$ SE
Central Crete								
R_{XZ}(TC) vs. D	19	0.907	−0.952	10.64 ± 0.47	1.04 ± 0.08	166.45/0.000	0.907	1.03 ± 0.02
R_{XZ}(MOE) vs. D	19	0.933	−0.966	11.42 ± 0.42	1.11 ± 0.07	238.57/0.000	0.933	1.11 ± 0.02
R_{XZ}(MRL) vs. D	19	0.918	−0.958	10.41 ± 0.43	1.02 ± 0.07	190.62/0.000	0.918	1.01 ± 0.02
West Crete B								
R_{XZ}(TC) vs. D	31	0.806	−0.898	12.95 ± 0.70	1.24 ± 0.11	120.27/0.000	0.804	1.29 ± 0.03
R_{XZ}(MOE) vs. D	31	0.837	−0.915	13.77 ± 0.67	1.32 ± 0.11	149.71/0.000	0.836	1.37 ± 0.03
R_{XZ}(MRL) vs. D	31	0.832	−0.912	12.66 ± 0.64	1.23 ± 0.10	142.99/0.000	0.832	1.24 ± 0.03
West Crete A								
R_{XZ}(TC) vs. D	32	0.823	−0.907	12.09 ± 0.68	1.21 ± 0.10	139.94/0.000	0.819	1.13 ± 0.03
R_{XZ}(MOE) vs. D	32	0.832	−0.912	13.18 ± 0.72	1.32 ± 0.11	148.77/0.000	0.828	1.23 ± 0.03
R_{XZ}(MRL) vs. D	32	0.819	−0.905	11.96 ± 0.68	1.20 ± 0.10	135.94/0.000	0.813	1.11 ± 0.03
South Peloponnese–Kythira								
R_{XZ}(TC) vs. D	32	0.918	−0.958	19.45 ± 0.66	1.88 ± 0.10	337.92/0.000	0.918	1.92 ± 0.04
R_{XZ}(MOE) vs. D	32	0.924	−0.961	20.01 ± 0.65	1.91 ± 0.10	367.91/0.000	0.922	1.99 ± 0.04
R_{XZ}(MRL) vs. D	32	0.912	−0.955	18.21 ± 0.64	1.74 ± 0.10	313.14/0.000	0.911	1.81 ± 0.04
Central Peloponnese								
R_{XZ}(MOE) vs. D	54	0.859	−0.927	12.41 ± 0.44	1.23 ± 0.07	319.08/0.000	0.858	1.18 ± 0.01
North Peloponnese								
R_{XZ}(MOE) vs. D	32	0.521	−0.722	9.05 ± 0.96	0.87 ± 0.15	32.75/0.000	0.521	0.89 ± 0.02

n, number of data; r^2, coefficient of determination; r, coefficient of correlation; SE, standard error; ANOVA, analysis of variance.

regression analysis. For the hypothesis $\beta = 0$, the significance probability (p values) corresponding to the computed F values is much less than 0.001 in all cases (Table 1), thus the null hypothesis is rejected. It should be noted that among different functions (exponential, power, etc.) Eq. (1) gives the highest coefficient of determination (r^2).

Three regression equations were obtained for each of the four new profiles using the R_{XZ} values estimated from the three *Rf-φ* methods (Fig. 6c–f; Table 1). The equations for the north and central Peloponnese are based on R_{XZ} values estimated from the MOE method only (Fig. 6a,b; Table 1). Equation (1) fits very well in five profiles (Fig. 6b–f) where the r^2 values range between 0.80 and 0.93 (Table 1). A relatively poor fit with r^2 of 0.52 is obtained in the north Peloponnese profile (Fig. 6a; Table 1). This may be related to the absence of strain data from the lowermost levels (0–100 m) of the shear zone which are not exposed. Note that the original data set of this profile is augmented with new strain results from four samples collected in the deeper exposed levels (100–200 m) of the zone (Fig. 6a).

In cases where three regression equations have been obtained for the same area, they are characterized by similar r^2 values (Table 1). Moreover, the curves obtained from the results of both the MRL and MOE methods fall within the 95% confidence interval of the curves based on TC estimates (Fig. 6c–f). The upper limits of these intervals commonly coincide with the curves describing MOE strains. In turn, curves of the MRL strains lay below and usually very close to those describing TC strains. These observations are in accordance with the findings from comparison between different finite strain methods (Fig. 4b,c) and imply that all methods can effectively describe the strain profiles.

5.2. Correlation between the regression coefficients

Independently from both the strain method used for getting profiles and the position of the profiles in the shear zone, the ratio of the regression coefficients α/β remains fairly constant (Table 1). It is striking that on a scatter graph of α versus β the data points define a straight line through the origin (Fig. 7a), which can be described by the regression equation:

$$\alpha = 10.25\beta \quad \left(r^2 = 0.999\right) \tag{2}$$

Considering that the coefficients of Eq. (1) represent the R_{XZ}-axis intercept (α) and the slope (β) of the regression lines in linear-log space, the above relationship (Eq. 2) implies that the expected R_{XZ} value at the base of the shear zone and the strain gradient ($\beta = \mathrm{d}R_{XZ}/\mathrm{d}\ln D$) always have constant proportionality. As illustrated in Fig. 7b, this is also the case for any projected distance from the basal thrust. From the same graph is also obvious that the profiles recording the higher strain values are accompanied by the higher strain gradients. The above observations enable us to assume that the strain profiles can be sufficiently described by an empirical function

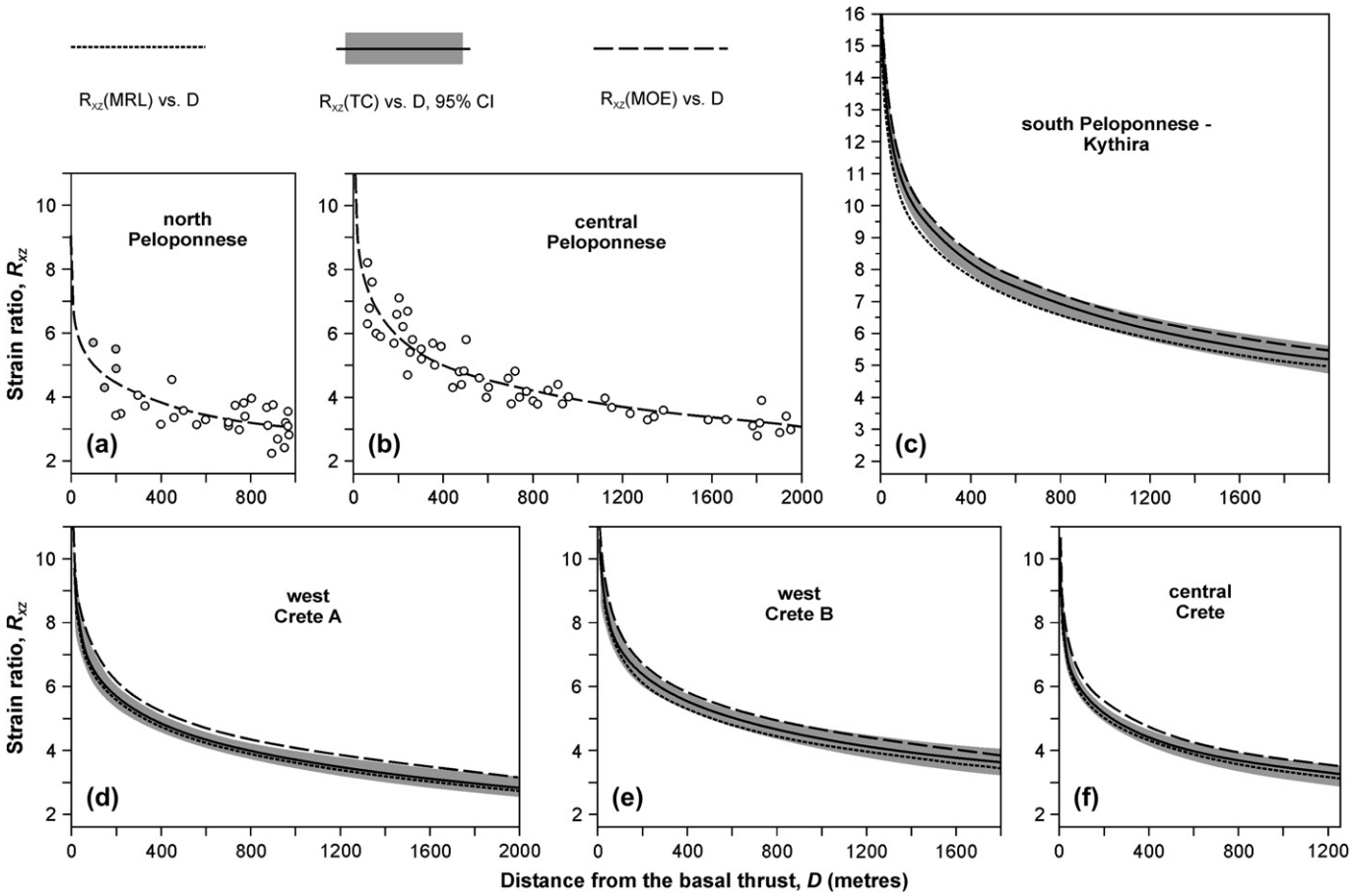

Fig. 6. Graphical representation of the regression equations obtained by fitting the logarithmic function $R_{XZ} = \alpha - \beta \ln D$ (Eq. 1) to the strain profiles from six areas in the studied shear zone. Data in (a) after Xypolias and Koukouvelas, 2001; in (b) after Xypolias and Kokkalas, 2006. The original data set of the north Peloponnese (a) has been augmented with new strain results from four samples (filled circles). Raw data of graphs in (c), (d), (e) and (f) are shown in Fig. 5 and listed in Appendix A. R_{XZ}(TC), R_{XZ}(MRL), R_{XZ}(MOE): strain ratios obtained by applying the TC, the MRL and the MOE methods, respectively. CI, confidence interval.

including only one varying parameter. Consequently substituting the value for α from Eq. (2) into Eq. (1) we have:

$$R_{XZ} = \beta(10.25 - \ln D) \tag{3}$$

The new regression equations, which resulted from the fitting of Eq. (3) to the data sets of all the profiles (Table 1), are practically identical to those obtained from the Eq. (1). In cases where three β values are estimated for the same area, they are restricted to a very small range (Table 1). This allows us to assume that each strain profile can be described by an average β value. Note that the coefficient values obtained from the MOE strains are 5.5% higher than the corresponding average β values. This finding was used to correct the new coefficients β of the strain profiles of the north and central Peloponnese, which are based on MOE estimates only. The average β values describing the corresponding six strain profiles, as well as the spatial variation of these along the shear zone, are illustrated in Fig. 8.

The spatial variation of coefficient β, in plan-view, shows a systematic increase of values from the tips to the centre of the shear zone (Fig. 8) implying the same spatial variation for the finite strain. Assuming a uniform distribution for the along-strike variation of β values, it seems that the centre of the shear zone is located ca. 50 km south-east from the south Peloponnese–Kythira transect (Fig. 8) and almost coincides with the crest of the parabolic curvature of the HP-belt. Although the observed strain pattern implies higher displacement in the centre of the shear zone, more data are needed to prove whether the shear zone was developed on a pre-existing or a contemporaneously formed curvature (e.g. Kwon and Mitra, 2004 and references therein).

6. Application to other natural examples

Finite-strain profiles from five ductile to semi-ductile thrust zones in the Alps, the Appalachians and the Himalaya were used to test whether the results outlined above have application to other natural examples (Fig. 9). All analysed profiles are characterized by a linear trend of the data points in linear $R_{XZ} - \log D$ space. For each case study, both Eq. (1) and Eq. (3) were fitted. Note that among different functions (linear, exponential, power etc), the proposed logarithmic functions give the highest r^2. The fit of the general function $R_{XZ} = \alpha - \beta \ln D$ (Eq. 1) indicates that the ratios α/β of regression coefficients

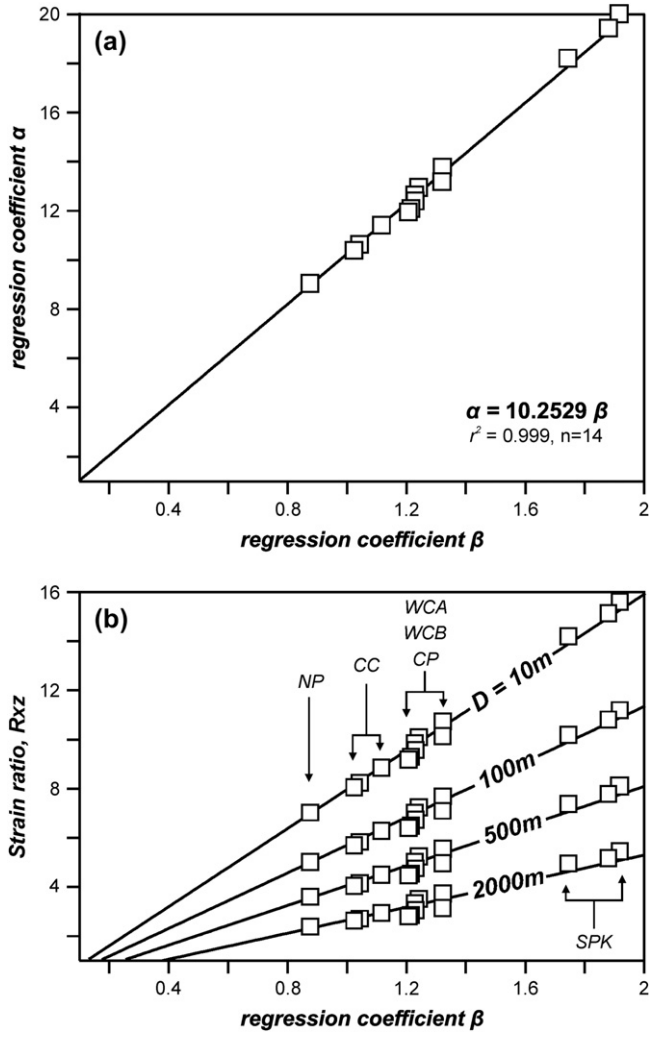

Fig. 7. (a) Plot showing correlation between the regression coefficients α and β obtained by fitting the equation $R_{XZ} = \alpha - \beta \ln D$ to the strain profiles. Values of coefficients are listed in Table 1. (b) Plot showing the relationship between strain ratio R_{XZ} and regression coefficients β from various distances, D, from the basal thrust. For a given distance (i.e. $D = 10$, 100, 500, 2000 m) from the basal thrust, the R_{XZ} and β values have constant proportionality in all the profiles. NP, north Peloponnese; CP, central Peloponnese; SPK, south Peloponnese–Kythira; WCA, west Crete A; WCB, west Crete B; CC, central Crete.

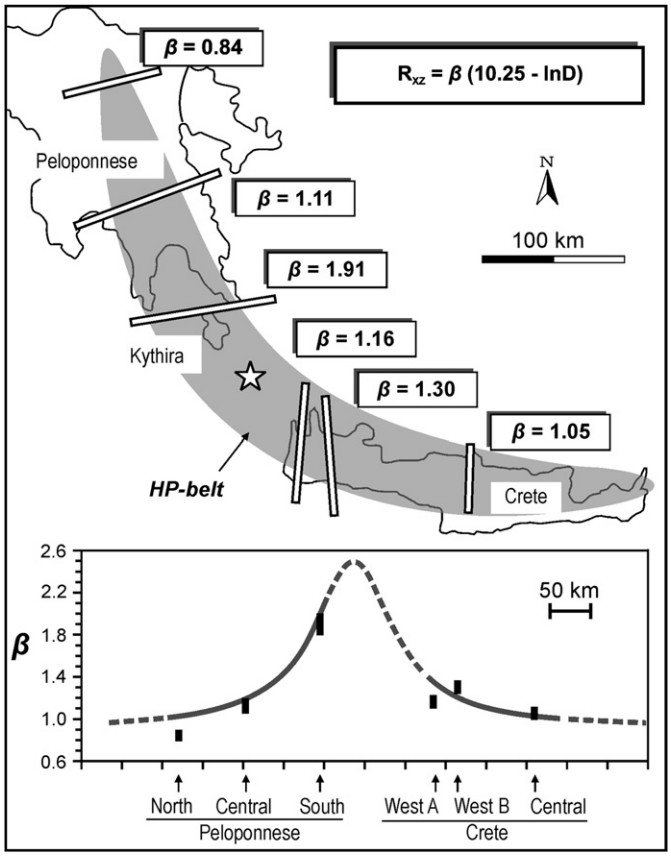

Fig. 8. Average β values describing the corresponding six strain profiles, and graph showing the variation, in map-view, of the β values from the tips to centre of the shear zone. The latter is located ca. 50 km south-east (star) of the South Peloponnese–Kythira transect.

are fairly constant and close to 10.25 (Fig. 9f) as also occurs in the studied shear zone (Fig. 7a). Below, we summarize the observations attempting to fit the empirical function $R_{XZ} = \beta(10.25 - \ln D)$ to each case study.

The Morcles Nappe in the western Helvetic Alps is potentially the most classical example of non-linear increase of finite strain toward a basal thrust (e.g. Ramsay, 1981). The nappe is also characterized by a steep horizontal gradient of increasing strain from the frontal part ($1 < R_{XZ} < 9$) to the root zone ($R_{XZ} > 50$) (Dietrich and Casey, 1989). The inferred down-section strain increase is clear in the strain profile recorded by Siddans (1983) within the frontal parts of the nappe (Fig. 9a). The proposed function fits very well ($r^2 = 0.8$) to this profile receiving a β value of 1 (Fig. 9a).

Across the Blue Ridge antiform in the central Appalachians the X/Z strain ratio also increases drastically close to major ductile thrust faults ($R_{XZ} \approx 6$) and then falls off to a nearly constant ($R_{XZ} \approx 2$) value (Mitra, 1979). This strain pattern generally depicts the shape of the proposed logarithmic curves (Fig. 10). Analysis of a strain profile across a major thrust fault reveals that the Eq. (3) sufficiently describes the observed strain pattern in both hanging wall and footwall of the thrust (Fig. 9b) with β values of 0.9 and 0.65, respectively.

The strain profile from the hanging wall of the North Mountain Thrust (central Appalachians) indicates a weak downward increase in R_{XZ} values from ca. 1.1 at the top to ca. 1.8 within 300 m of the basal thrust (Fig. 9c; Evans and Dunne, 1991). A relatively poor fit ($r^2 = 0.54$) of the logarithmic function to the profile was found in this example. This is possibly related to the absence of strain data from the lowermost levels of the thrust sheet. However, the obtained regression equation (Fig. 9c) with a β value of 0.35 is in line with observations for a markedly finite strain increase within an average of 46 m of the thrust fault (Dean and Kulander, 1972).

Cashman (1988) proposed a linear equation with $r^2 = 0.56$ for describing the strain variation in the footwall block of the Orlean Thrust in Klamath Mountains of California. Here, the

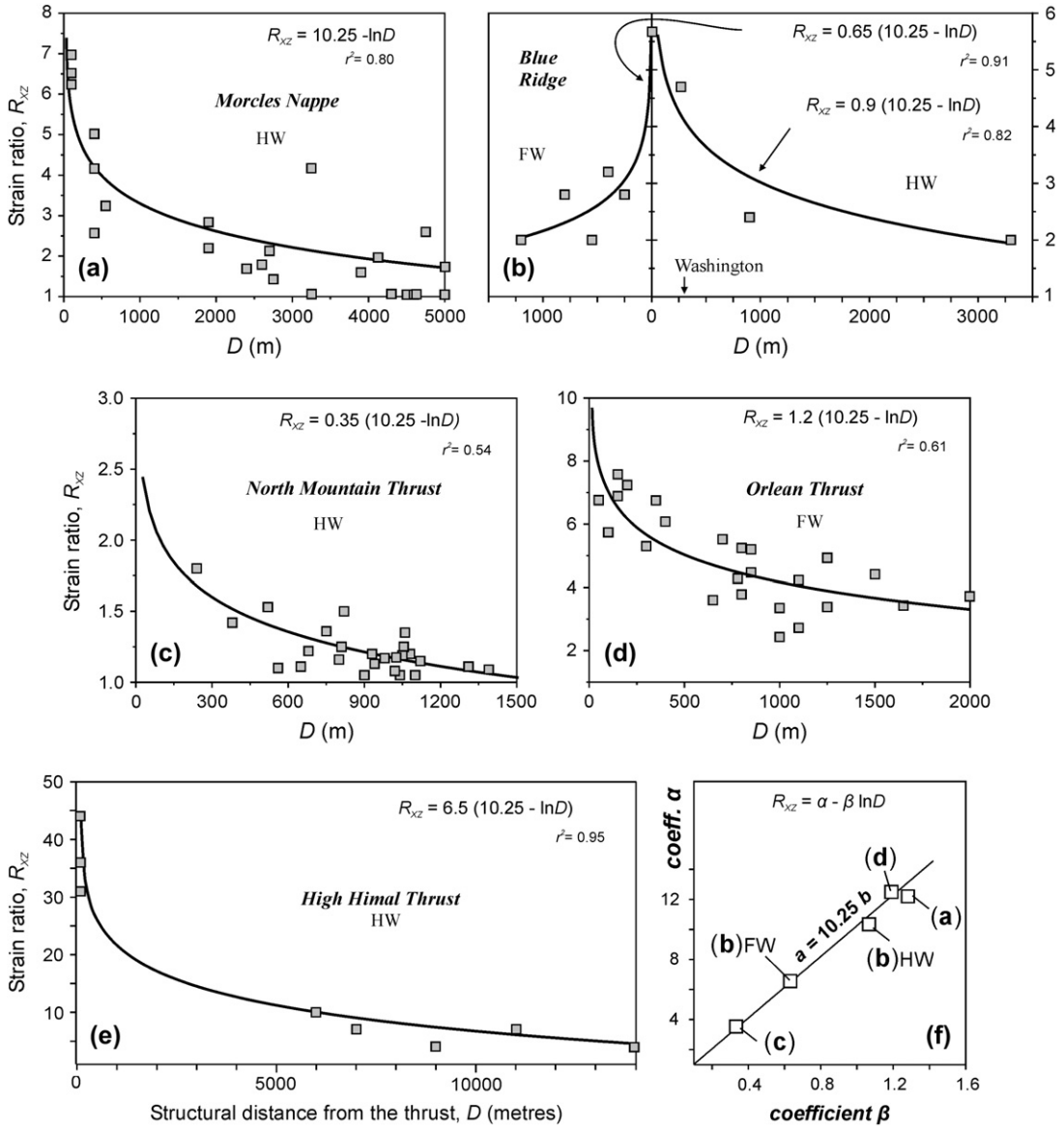

Fig. 9. Application of the proposed empirical function $R_{XZ} = \beta\ (10.25 - \ln D)$ (Eq. 3) to other natural occurring zones of ductile to semi-ductile thrusting. Data for the Morles Nappe (a) after Siddans (1983; his fig. 3); for the Blue Ridge (b) after Mitra (1979; his fig. 20); for the North Mountain Thrust (c) after Evans and Dunne (1991; their fig. 13); for the Orlean Thrust (d) after Cashman (1988); for the High Himal Thrust (e) after Goscombe et al. (2006; their fig. 11a). (f) Plot showing the correlation between the regression coefficients α and β obtained by fitting the equation $R_{XZ} = \alpha - \beta \ln D$ (Eq. 1) to the examples (a), (b), (c) and (d). FW, footwall; HW, hanging wall.

strain pattern is characterized by a systematic increase of R_{XZ} values from ca. 3.5 at a structural distance of 2 km below the thrust to ca. 7 adjacent to it (Fig. 9d). Our analysis indicated that the logarithmic Eq. (1) fits better to the dataset with $r^2 = 0.62$ and β value of 1.2 (Fig. 9d).

The distribution of ductile strain above the Kakhtang or High Himal Thrust (Goscombe et al., 2006 and references therein), which occurs within the Greater Himalayan Sequence in eastern Nepal, can also be described by the proposed Eq. (3). The overall strain pattern, which is characterized by extremely high strain ratios of 30–45 into the mylonitic zone (100–400 m wide) of the thrust and a relatively homogeneous strain distribution with strain ratios of 4–10 at progressively higher structural levels (Goscombe et al., 2006; Fig. 9e), is fairly well described by a β value of 6.5. Here, the results of regression analysis (Fig. 9e) are indicative due to significant uncertainty in the distance estimates.

The above-mentioned examples indicate that the empirical Eq. (3) sufficiently describes the finite strain profiles of other naturally occurring zones of ductile to semi-ductile thrusting. The graphical representation of Eq. (3) for various β values shows that the opening angle of the curves increases with β (Fig. 10). This implies that thrust-sense shear zones or sheets of relatively low strain (low β) are characterized by extreme strain localization at their base. At progressively higher strain levels (higher β) deformation tends to become less localized.

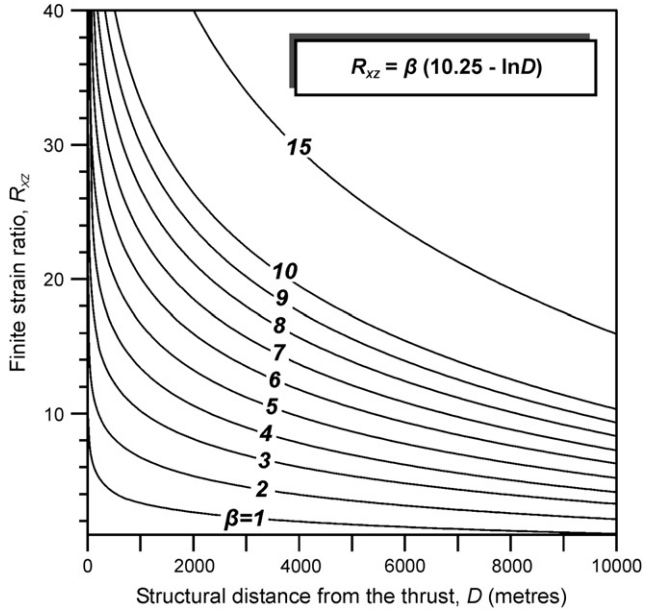

Fig. 10. Graphical representation of the proposed empirical correlation function (Eq. 3) between strain ratio and structural distance from a basal thrust for various β values. The coefficient β ($= dR_{XZ}/d\ln D$) represents the strain gradient.

7. Conclusions

Application of three strain analysis methods (the theta-curve, the mean object ellipse and the mean radial length method) in 120 samples from a crustal-scale zone of ductile thrusting in the External Hellenides reveals that all methods give very consistent results. Finite strain profiles across the shear zone, which are based on these results, indicate a non-linear increase of R_{XZ} strain values with proximity to the basal thrust. In all profiles the observed strain variation with distance, D, from the basal thrust obeys a simple logarithmic function of the form: $R_{XZ} = \beta(10.25 - \ln D)$, where β is the strain gradient in linear $R_{XZ} - \ln D$ space (Fig. 10). This function implies that thrust zones with low β values are characterized by relatively low and extremely localized strain at their base. Greater and more widely distributed strain occurs in zones with high β values.

The above empirical function sufficiently describes the finite strain profiles of naturally occurring zones of ductile to semi-ductile thrusting in other orogenic belts such as the Alps, the Appalachians and Himalaya. Although more examples are needed to test the descriptive power of the proposed function, it could be used as a tool for obtaining strain profiles in zones of ductile thrusting where detailed finite strain analysis is not possible.

Acknowledgments

The manuscript benefited significantly from constructive reviews of Kieran F. Mulchrone and Daniel Tatham, and thoughtful suggestions made by Rick Law. V.C. acknowledges the receipt of research scholarship from the IKY (Greek State Scholarships Foundation).

Appendix. A

Sample	Longitude	Latitude	D (m)	n	TC method		MOE method		MRL method		Fry method
					R_{XZ}	χ^2	R_{XZ}	Er	R_{XZ}	Er	R_{XZ}
South Peloponnese–Kythira											
KY25	22°57′27″	36°21′40″	1980	89	4.99	13.2	5.40	0.58	5.09	0.35	–
KY9a	22°58′14″	36°20′09″	1950	109	4.59	22.6	4.62	0.42	4.35	0.23	–
NE17	23°05′45″	36°29′16″	1920	174	5.25	16.1	5.95	0.48	5.50	0.29	–
NE6	23°05′15″	36°31′50″	1900	176	4.69	17.7	5.08	0.45	4.36	0.28	5.16
NE16	23°05′40″	36°29′12″	1880	178	5.40	9.5	6.21	0.66	5.49	0.33	–
KY8b	22°57′56″	36°20′33″	1850	91	4.96	12.4	4.91	0.47	4.80	0.34	–
NE19	23°04′10″	36°29′52″	1830	143	5.85	12.6	6.56	0.50	6.23	0.33	–
NE9	23°04′46″	36°32′02″	1800	248	5.15	13.0	5.65	0.50	5.06	0.20	–
KY10	22°58′19″	36°19′38″	1800	79	5.35	9.2	5.72	0.53	5.10	0.34	–
NE11	23°04′39″	36°32′02″	1770	155	4.65	25.0	4.95	0.46	4.39	0.26	–
NE18	23°04′28″	36°30′30″	1750	172	4.95	9.5	5.29	0.48	4.48	0.25	–
KY15a	22°57′47″	36°18′41″	1750	81	5.96	7.2	6.45	0.58	5.87	0.46	–
NE12	23°04′22″	36°31′54″	1720	67	5.89	1.4	6.30	0.61	5.74	0.49	–
KY7	22°57′23″	36°20′49″	1600	46	5.18	0.7	5.65	0.44	5.07	0.46	–
KY34	22°56′60″	36°18′24″	1400	136	5.34	14.7	5.31	0.51	4.69	0.41	–
KY33	22°56′38″	36°18′29″	1350	95	6.25	13.0	6.24	0.62	5.68	0.38	–
KY36	22°56′36″	36°19′26″	1200	223	6.03	24.1	5.78	0.71	5.30	0.32	–
KY6	22°56′57″	36°20′03″	1100	101	6.70	6.1	6.85	0.57	6.31	0.42	–
KY23	22°55′36″	36°19′16″	1000	50	7.00	4.1	7.37	0.68	6.84	0.55	–
KY31	22°55′56″	36°19′59″	900	146	6.90	11.2	6.81	0.65	6.23	0.37	–
KY5	22°56′13″	36°19′45″	850	57	6.23	8.4	6.51	0.52	5.88	0.47	–

(*continued on next page*)

Appendix. A (*continued*)

Sample	Longitude	Latitude	*D* (m)	*n*	TC method		MOE method		MRL method		Fry method
					R_{XZ}	χ^2	R_{XZ}	Er	R_{XZ}	Er	R_{XZ}
KY19	22°55′04″	36°20′47″	800	167	6.54	21.5	6.32	0.70	5.53	0.38	–
KY13	22°54′45″	36°18′30″	600	112	8.23	16.7	8.26	0.83	7.79	0.45	–
MA3	22°27′52″	36°26′55″	130	115	11.40	23.8	11.26	0.94	10.33	0.77	–
MA5	22°27′47″	36°26′39″	100	158	12.38	14.8	12.85	0.85	12.18	0.82	–
MA8	22°28′59″	36°25′46″	80	135	10.55	17.3	10.93	0.88	10.21	0.83	–
MA2b	22°27′54″	36°26′59″	70	113	10.41	21.4	11.93	0.87	10.36	0.72	–
MA7	22°29′01″	36°25′43″	70	136	14.6	21.4	14.61	0.77	13.24	0.91	–
MA2a	22°27′55″	36°27′00″	50	121	13.15	22.9	13.06	0.85	11.48	0.71	–
MA6	22°28′58″	36°25′47″	40	50	11.37	5.4	11.98	0.99	10.91	0.90	–
MA1	22°27′57″	36°27′03″	15	183	13.95	24.7	14.97	0.97	13.84	0.71	–
MA9	22°28′53″	36°25′43″	10	92	13.22	13.1	13.38	0.86	12.10	0.94	–
MA10	22°27′52″	36°26′50″	−10	309	5.71	24.5	6.01	0.64	5.28	0.29	–
MA13	22°27′08″	36°27′24″	−70	211	5.70	11.0	6.24	0.78	5.52	0.33	–
MA11a	22°26′54″	36°27′29″	−120	288	5.60	5.1	6.29	0.58	5.56	0.33	–
MA11b	22°26′41″	36°27′34″	−130	312	5.90	26.8	6.69	0.67	5.86	0.31	–
MA12	22°27′25″	36°27′22″	−130	342	4.15	24.4	4.64	0.59	4.41	0.24	–
MA14	22°26′41″	36°27′37″	−150	41	6.40	0.9	6.88	0.67	6.41	0.85	–
West Crete A											
CR241	23°35′41″	35°27′21″	1970	69	2.75	9.1	2.95	0.24	2.57	0.14	–
CG990	23°36′33″	35°26′07″	1950	179	2.31	18.8	2.55	0.25	2.20	0.02	–
CR238	23°36′29″	35°26′16″	1900	205	2.85	19.1	3.22	0.30	2.86	0.17	–
CG314	23°38′10″	35°25′10″	1900	345	2.89	10.8	3.29	0.32	2.97	0.14	3.14
CR231	23°38′42″	35°24′58″	1880	42	2.80	4.6	3.10	0.27	2.74	0.23	–
CG310	23°38′43″	35°24′56″	1880	147	3.40	11.6	3.27	0.54	3.32	0.04	–
CR232	23°38′41″	35°24′55″	1850	256	5.54	15.4	6.05	0.62	5.39	0.25	–
CR58	23°37′32″	35°24′17″	1800	149	2.98	26.7	3.21	0.29	2.98	0.16	–
CR11	23°32′51″	35°23′34″	1750	100	2.52	11.6	2.94	0.30	2.69	0.23	–
CR4	23°37′16″	35°23′52″	1580	223	2.77	14.8	3.08	0.34	2.84	0.16	–
CG3	23°39′59″	35°16′18″	1450	163	3.05	20.4	3.15	0.48	2.75	0.20	3.42
CR209	23°39′57″	35°16′17″	1450	345	2.46	19.5	2.88	0.28	2.38	0.10	2.58
CR1	23°40′00″	35°16′29″	1330	32	3.48	3.6	4.02	0.46	3.44	0.37	–
CR2	23°39′35″	35°16′41″	1320	243	2.42	15.0	2.76	0.35	2.42	0.09	–
CR48	23°39′47″	35°24′22″	1200	146	3.54	15.3	3.90	0.34	3.44	0.22	–
CR6	23°41′19″	35°16′04″	1100	154	4.95	25.0	5.48	0.52	4.85	0.25	–
CR56	23°34′28″	35°23′49″	1020	286	4.27	12.2	4.64	0.41	4.07	0.19	–
CG40	23°40′53″	35°18′31″	1000	110	3.45	7.0	3.82	0.32	3.37	0.24	–
CR25	23°44′12″	35°17′13″	970	187	3.25	5.9	3.58	0.37	3.16	0.19	3.40
CG12	23°38′09″	35°17′59″	850	80	3.55	10.1	3.81	0.23	3.42	0.31	3.78
CR15	23°34′35″	35°23′32″	850	77	4.39	13.8	4.82	0.51	4.33	0.34	–
CR16	23°34′31″	35°23′23″	800	98	3.53	9.6	4.08	0.35	3.25	0.30	3.31
CR35	23°33′52″	35°23′05″	770	152	4.75	3.0	5.43	0.62	5.20	0.38	4.93
CR22	23°38′17″	35°18′23″	650	180	4.50	17.5	4.50	0.40	4.34	0.21	4.09
CR21	23°38′39″	35°18′48″	550	210	5.15	15.5	5.41	0.71	4.93	0.26	–
CR36	23°36′10″	35°21′44″	470	322	4.60	7.5	5.22	0.54	4.75	0.21	4.40
CR47	23°37′43″	35°22′01″	330	95	5.85	11.8	6.58	0.46	5.83	0.32	5.29
CR20	23°39′15″	35°19′42″	200	136	6.90	13.7	7.30	0.69	6.62	0.36	–
CG961	23°35′57″	35°20′47″	100	50	8.00	3.8	8.60	0.91	7.57	0.77	–
CR218	23°35′52″	35°20′47″	80	206	5.05	23.0	5.50	0.60	4.84	0.27	–
CR217	23°35′39″	35°20′43″	70	128	6.80	18.5	7.22	0.63	6.84	0.40	–
CR214	23°36′01″	35°19′08″	50	340	6.60	27.0	7.16	0.90	6.29	0.24	–
CR213	23°35′47″	35°19′17″	20	136	8.12	18.4	9.20	0.90	8.46	0.69	–
West Crete B											
CR59	23°43′59″	35°24′40″	1800	57	3.78	10.9	3.89	0.42	3.43	0.29	–
CR228	23°44′01″	35°24′36″	1750	50	3.91	3.5	4.10	0.10	3.57	0.29	–
CR243	23°44′07″	35°24′27″	1650	87	3.12	10.2	3.54	0.40	3.18	0.32	–
CR172	23°44′00″	35°24′15″	1520	213	4.55	19.7	5.07	0.69	4.49	0.22	–
CR245	23°46′07″	35°24′31″	1480	152	4.30	16.7	4.55	0.41	4.08	0.26	–
CR37	23°44′05″	35°24′12″	1350	103	3.87	12.6	4.21	0.56	3.78	0.33	–
CR38	23°44′02″	35°24′01″	1200	206	3.57	24.6	3.94	0.38	3.62	0.15	–
CR246	23°42′24″	35°23′57″	1150	134	4.46	22.1	4.61	0.33	4.23	0.39	–
CR39	23°44′00″	35°23′48″	1000	117	4.90	17.8	4.95	0.53	4.52	0.39	–
CR40	23°43′55″	35°23′41″	950	181	3.89	20.5	4.09	0.52	3.57	0.19	–

Appendix. A (*continued*)

Sample	Longitude	Latitude	*D* (m)	*n*	TC method		MOE method		MRL method		Fry method
					R_{XZ}	χ^2	R_{XZ}	Er	R_{XZ}	Er	R_{XZ}
CR60	23°43′56″	35°23′42″	800	98	5.50	13.7	5.38	0.60	4.92	0.43	–
CR66	23°51′02″	35°24′10″	780	91	4.50	7.8	4.52	0.36	4.27	0.25	–
CR26	23°47′29″	35°18′10″	700	75	4.50	13.6	4.94	0.46	4.62	0.22	–
CR27	23°49′30″	35°19′32″	630	218	4.05	15.8	4.58	0.43	4.11	0.19	4.05
CR186	23°49′47″	35°24′19″	620	133	5.04	18.1	5.28	0.55	4.89	0.3	–
CR61	23°43′55″	35°22′56″	570	175	4.55	27.3	5.05	0.62	4.45	0.27	4.48
CR89	23°49′33″	35°21′23″	500	209	5.12	24.0	5.70	0.52	5.01	0.22	–
CR90	23°49′07″	35°21′32″	400	226	4.22	22.6	4.41	0.47	4.10	0.18	–
CR180	23°53′44″	35°23′17″	400	107	6.11	13.3	6.01	0.59	5.38	0.36	–
CR187	23°49′15″	35°25′14″	350	176	6.15	10.4	6.80	0.61	6.13	0.34	–
CR72	23°56′36″	35°25′22″	330	229	4.55	19.8	4.85	0.55	4.21	0.24	–
CR80	23°51′51″	35°23′54″	320	79	5.60	12.2	6.15	0.43	5.34	0.3	–
CR78	23°53′30″	35°25′50″	300	122	6.50	16.8	6.99	0.56	6.22	0.26	6.94
CR181	23°53′33″	35°22′20″	300	225	7.38	26.3	7.42	0.56	7.23	0.37	–
CR87	23°56′49″	35°25′37″	270	92	6.10	13.6	6.10	0.46	5.71	0.3	5.82
CR94	23°48′55″	35°19′26″	180	136	7.16	23.8	7.95	0.80	7.16	0.35	–
CR106	23°47′10″	35°21′36″	120	167	6.41	14.3	6.81	0.55	6.15	0.43	–
CR28	23°50′45″	35°21′09″	80	161	7.11	8.5	7.94	0.78	6.99	0.47	6.5
CR76	23°54′03″	35°22′41″	70	205	7.72	9.3	8.52	0.88	7.60	0.47	–
CR92	23°48′13″	35°18′58″	50	193	9.53	27.1	9.62	0.97	8.84	0.47	–
CR81	23°52′02″	35°22′58″	20	121	8.42	24.9	8.92	0.78	8.41	0.64	–
Central Crete											
CR116	24°58′09″	35°24′03″	1250	207	2.66	17.7	3.06	0.28	2.73	0.13	2.45
CR123	24°58′56″	35°21′55″	1220	162	3.75	24.0	4.03	0.41	3.70	0.22	–
CR115	24°57′51″	35°24′14″	1100	142	3.59	15.6	3.48	0.32	3.20	0.23	–
CR119	24°57′54″	35°24′02″	980	189	3.35	21.1	3.66	0.41	3.27	0.15	–
CR132	24°54′20″	35°24′16″	830	133	3.24	9.2	3.56	0.30	3.19	0.28	–
CR118	24°57′28″	35°24′06″	800	127	4.25	13.3	4.67	0.53	4.19	0.37	–
CR107	24°46′36″	35°25′02″	680	156	3.99	7.3	4.26	0.53	3.83	0.25	–
CR136	24°55′23″	35°24′03″	520	173	4.71	11.7	5.14	0.52	4.57	0.29	–
CR109	24°46′50″	35°25′01″	420	62	3.95	13.5	4.15	0.35	3.64	0.24	–
CR127	24°58′01″	35°21′18″	380	268	4.30	26.0	4.79	0.48	4.23	0.20	–
CR113	24°56′56″	35°23′43″	300	147	5.34	18.9	5.47	0.55	5.30	0.27	5.78
CR114	24°56′57″	35°23′40″	300	301	4.10	17.8	4.63	0.44	4.09	0.17	–
CR131	24°52′08″	35°24′34″	250	50	4.45	5.8	4.76	0.61	4.19	0.46	–
CR133	24°54′04″	35°23′55″	180	219	5.20	13.4	5.91	0.63	5.34	0.29	–
CR125	24°57′50″	35°21′36″	170	104	7.25	3.4	7.38	0.86	7.35	0.49	6.78
CR112	24°56′05″	35°23′20″	130	125	5.65	21.3	5.78	0.75	5.16	0.33	–
CR110	24°51′27″	35°24′14″	100	185	5.35	2.4	6.05	0.46	5.53	0.27	–
CR111	24°55′16″	35°23′31″	50	172	6.76	4.5	7.33	0.66	6.72	0.41	–
CR135	24°54′01″	35°23′40″	20	350	6.90	9.0	7.71	0.90	7.03	0.34	–
CR134	24°54′01″	35°23′44″	10	144	8.96	7.2	9.27	0.87	8.40	0.55	–

D, distance from the basal thrust; R_{XZ}, finite strain ratio in *XZ* sections; *n*, number of analysed strain markers; Er, error; TC, theta-curve; MOE, mean object ellipse; MRL, mean radial length.

References

Arbaret, L., Burg, J.-P., 2003. Complex flow in lowest crustal, anastomosing mylonites: Strain gradients in a Kohistan gabbro, northern Pakistan. Journal of Geophysical Research 108 (B10). ETG 4-1-ETG 4–18.

Avigad, D., Garfunkel, Z., Jolivet, L., Azañón, J.M., 1997. Back arc extension and denudation of Mediterranean eclogites. Tectonics 16, 924–941.

Baumann, A., Best, G., Gwosdz, W., Wachendorf, H., 1976. The nappe pile of eastern Crete. Tectonophysics 30, T33–T40.

Blumör, T., 1998. Die Phyllit-Quartzit-Serie SE-Lakoniens (Peloponnes, Griechenland): Hochdruckmetamorphite in einem orogenen Keil. Frankfurter Geowissenschaftiche Arbeiten 17, 1–187.

Burg, J.-P., 1999. Ductile structures and instabilities: their implication for Variscan tectonics in the Ardennes. Tectonophysics 309, 1–25.

Burg, J.-P., Laurent, P., 1978. Strain analysis of a shear-zone in a granodiorite. Tectonophysics 47, 15–42.

Butler, R.W.H., Casey, M., Lloyd, G.E., Bond, C.E., McDade, P., Shipton, Z., Jones, R., 2002. Vertical stretching and crustal thickening at Nanga Parbat, Pakistan Himalaya: A model for distributed continental deformation during mountain building. Tectonics 21. 9-1-9-17.

Carreras, J., 2001. Zooming on Northern Cap de Creus shear zones. Journal of Structural Geology 23, 1457–1486.

Cashman, S.M., 1988. Finite-strain patterns of Nevadan deformation, western Klamath Mountains, California. Geology 16, 839–843.

Chatzaras, V., Xypolias, P., Doutsos, T., 2006. Exhumation of high-pressure rocks under continuous compression: a working hypothesis for southern Hellenides (central Crete, Greece). Geological Magazine 143, 859–876.

Chew, D.M., 2003. An Excel spreadsheet for finite strain analysis using the Rf-φ technique. Computers & Geosciences 29, 795–799.

Dean, S.L., Kulander, B.R., 1972. Oolite deformation associated with faulting in the northern Shenandoah Valley. In: Lessing, P., Hayhurst, R.I., Barlow, J.A., Woodfork, L.D. (Eds.), Appalachian Structures: Origin, Evolution, and Possible Potential for New Exploraton Frontiers. West Virginia Geological Survey, pp. 72–90.

Dietrich, D., Casey, M., 1989. A new tectonic model for the Helvetic nappes. In: Coward, M.P., Dietrich, D., Park, R.G. (Eds.), Alpine Tectonics. Geological Society, London, Special Publications, vol. 45, pp. 47–63.

Dittmar, D., Meyer, W., Oncken, O., Schievenbusch, T., Walter, R., Von Winterfeld, C., 1994. Strain partitioning across a fold and thrust belt: the Rhenish Massif, Mid European Variscides. Journal of Structural Geology 16, 1335–1352.

Doutsos, T., Koukouvelas, I., Poulimenos, G., Kokkalas, S., Xypolias, P., Skourlis, K., 2000. An exhumation model of the south Peloponnesus, Greece. International Journal of Earth Science 89, 350–365.

Doutsos, T., Koukouvelas, I.K., Xypolias, P., 2006. A new orogenic model for the External Hellenides. In: Robertson, A.H.F., Mountrakis, D. (Eds.), Tectonic Development of the Eastern Mediterranean region. Geological Society, London, Special Publications, vol. 260, pp. 507–520.

Dutruge, G., Burg, J.-P., 1997. Strain localisation in an orthogneiss laccolith (the Pinet Massif, Aveyron, southern France). Tectonophysics 280, 47–60.

Dutruge, G., Burg, J.-P., Lapierre, J., Vigneresse, J.-L., 1995. Shear strain analysis and periodicity within shear gradients of metagranite shear zones. Journal of Structural Geology 17, 819–830.

Erslev, E.A., Ge, H., 1990. Least-squares center-to-center and mean object ellipse fabric analysis. Journal of Structural Geology 12, 1047–1059.

Evans, M.A., Dunne, W.M., 1991. Strain factorization and partitioning in the North Mountain thrust sheet, central Appalachians, U.S.A. Journal of Structural Geology 13, 21–35.

Feldhoff, R.A., Lücke, A., Richter, D.K., 1991. Über die Diagenese-Metamorphosebedingugen der Pindos- und Tripolitza-Serie auf der Insel Kreta (Griechenland). Zentralblatt für Geologie und Paläontologie Teil I-11, 1611–1622.

Fry, N., 1979. Random point distributions and strain measurement in rocks. Tectonophysics 60, 89–105.

Fusseis, F., Handy, M.R., Schrank, C., 2006. Networking of shear zones at the brittle-to-viscous transition (Cap de Creus, NE Spain). Journal of Structural Geology 28, 1228–1243.

Goscombe, B., Gray, D., Hand, M., 2006. Crustal architecture of the Himalayan metamorphic front in eastern Nepal. Gondwana Research 10, 232–255.

Grasemann, B., Fritz, H., Vannay, J.C., 1999. Quantitative kinematic flow analysis from the Main Central Thrust Zone (NW-Himalaya, India): implications for a decelerating strain path and the extrusion of orogenic wedges. Journal of Structural Geology 21, 837–853.

Gray, D.R., Willman, C.E., 1991. Thrust-related strain gradients and thrusting mechanisms in a chevron-folded sequence, southeastern Australia. Journal of Structural Geology 13, 691–710.

Greiling, R., 1982. The metamorphic and structural evolution of the Phyllite–Quartzite Nappe of western Crete. Journal of Structural Geology 4, 291–297.

Hirth, G., Tullis, J., 1992. Dislocation creep regimes in quartz aggregates. Journal of Structural Geology 14, 145–159.

Horsman, E., Tikoff, B., 2007. Constraints on deformation path from finite strain gradients. Journal of Structural Geology 29, 256–272.

Katagas, C., Tsolis-Katagas, P., Baltatzis, E., 1991. Chemical mineralogy and illite crystallinity in low grade metasediments, Zarouchla Group, Northern Peloponnesus, Greece. Mineralogy and Petrology 44, 57–71.

Kokkalas, S., Doutsos, T., 2004. Kinematics and strain partitioning in the southeast Hellenides (Greece). Geological Journal 39, 121–140.

Kokkalas, S., Xypolias, P., Koukouvelas, I.K., Doutsos, T., 2006. Post-collisional contractional and extensional deformation in the Aegean region. In: Dilek, Y., Pavlides, S. (Eds.), Post-Collisional Tectonics and Magmatism in the Eastern Mediterranean Region. Special Papers, 409. Geological Society of America, pp. 97–123.

Kowalczyk, G., Richter, D., Risch, H., Winter, P., 1977. Zur zeitlichen Einstufung der tektogenetischen Ereignisse auf dem Peloponnes (Griechenland). Neues Jahrbuch für Geologie und Paläontologie, Monatshefte 1977, 549–564.

Kwon, S., Mitra, G., 2004. Strain distribution, strain history, and kinematic evolution associated with the formation of arcuate salients in fold-thrust belts: The example of the Provo salient, Sevier orogen, Utah. In: Sussman, A.J., Weil, A.B. (Eds.), Orogenic Curvature. Special Papers, 383. Geological Society of America, pp. 205–223.

Law, R.D., 1986. Relationships between strain and quartz crystallographic fabrics in the Roche Maurice quartzites of Plougastel, western Brittany. Journal of Structural Geology 8, 493–515.

Lisle, R.J., 1977. Clastic grain shape and orientation in relation to cleavage from the Aberystwyth Grits, Wales. Tectonophysics 39, 381–395.

Lisle, R.J., 1985. Geometrical Strain Analysis, A Manual for the Rf-φ Technique. Pergamon Press, Oxford.

Lisle, R.J., 1994. Palaeostrain analysis. In: Hancock, P.L. (Ed.), Continental Deformation. Pergamon Press, Oxford, pp. 28–42.

Merle, O., 1989. Strain models within spreading nappes. Tectonophysics 124, 211–222.

Mitra, G., 1979. Ductile deformation zones in Blue Ridge basement rocks and estimation of finite strains. Geological Society of America Bulletin 90, 935–951.

Mulchrone, K.F., 2005. An analytical error for the mean radial length method of strain analysis. Journal of Structural Geology 27, 1658–1665.

Mulchrone, K.F., Meere, P.A., 2001. Windows program for the analysis of tectonic strain using deformed elliptical markers. Computers and Geosciences 27, 1251–1255.

Mulchrone, K.F., O'Sullivan, F., Meere, P.A., 2003. Finite strain estimation using the mean radial length of elliptical objects with bootstrap confidence intervals. Journal of Structural Geology 25, 529–539.

Mulchrone, K.F., Meere, P.A., Roy Choudhury, K., 2005. SAPE: a program for semi-automatic parameter extraction for strain analysis. Journal of Structural Geology 27, 2084–2098.

Onasch, C.M., 1984. Application of the Rf-φ technique to elliptical markers deformed by pressure solution. Tectonophysics 110, 157–165.

Passchier, C.W., 1998. Monoclinic model shear zones. Journal of Structural Geology 20, 1121–1137.

Ramsay, J.G., 1980. Shear zone geometry: a review. Journal of Structural Geology 2, 83–99.

Ramsay, J.G., 1981. Tectonics of the Helvetic Nappes. In: McClay, K.R., Price, N.J. (Eds.), Thrust and Nappe Tectonics. Geological Society, London, Special Publications, vol. 9, pp. 293–309.

Ramsay, J.G., Graham, R.H., 1970. Strain variation in shear belts. Canadian Journal of Earth Sciences 7, 786–813.

Ramsay, J.G., Huber, M.I., 1983. The Techniques of Modern Structural Geology. In: Strain Analysis, Vol. 1. Academic Press, London.

Ring, U., Reischmann, T., 2002. The weak and superfast Cretan detachment, Greece: exhumation at subduction rates in extruding wedges. Journal of the Geological Society, London 159, 225–228.

Robertson, A.H.F., 2006. Sedimentary evidence from the south Mediterranean region (Sicily, Crete, Peloponnese, Evia) used to test alternative models for the regional tectonic setting of Tethys during Late Palaeozoic-Early Mesozoic time. In: Robertson, A.H.F., Mountrakis, D. (Eds.), Tectonic Development of the Eastern Mediterranean region. Geological Society, London, Special Publications, vol. 260, pp. 91–154.

Sanderson, D.J., 1982. Models of strain variation in nappes and thrust sheets: a review. Tectonophysics 88, 201–233.

Schwarz, S., Stöckhert, B., 1996. Pressure solution in siliciclastic HP-LT metamorphic rocks—constraints on the state of stress in deep levels of accretionary complexes. Tectonophysics 255, 203–209.

Seidel, E., Kreuzer, H., Harre, W., 1982. A late Oligocene/early Miocene high pressure belt in the external Hellenides. Geologische Jahrbuch E23, 165–206.

Siddans, A.W.B., 1983. Finite strain patterns in some Alpine nappes. Journal of Structural Geology 5, 441–448.

Sørensen, K., 1983. Growth and dynamics of the Nordre Stromfjord shear zone. Journal of Geophysical Research 88 (B4), 3419–3437.

Theye, T., Seidel, E., Vidal, O., 1992. Carpholite, sudoite, and chloritoid in low-grade high-pressure metapelites from Crete and the Peloponnese. European Journal of Minerology 4, 487–507.

Thomson, S.N., Stöckhert, B., Rauche, H., Brix, M.R., 1998. Thermochronology of the high-pressure metamorphic rocks of Crete, Greece: implications for the speed of tectonic processes. Geology 26, 259–262.

Williams, G.D., Chapman, T.J., Milton, N.J., 1984. Generation and modification of finite strain patterns by progressive thrust faulting in the Laksefjord Nappe, Finnmark. Tectonophysics 107, 177–186.

Wilson, C.J.L., 1982. Foliation in Quartz Mylonite. In: Borradaile, G.J., Bayly, M.B., Powell, C.Mc.A (Eds.), Atlas of Deformational and Metamorphic Rock Fabrics. Springer, Berlin, pp. 340–341.

Xypolias, P., Doutsos, T., 2000. Kinematics of rock flow in a crustal-scale shear zone: implication for the orogenic evolution of the southwestern Hellenides. Geological Magazine 137, 81–96.

Xypolias, P., Kokkalas, S., 2006. Heterogeneous ductile deformation along a mid-crustal extruding shear zone: an example from the External Hellenides (Greece). In: Law, R.D., Searle, M., Godin, L. (Eds.), Channel Flow, Ductile Extrusion and Exhumation in Continental Collision Zones. Geological Society, London, Special Publications, vol. 268, pp. 497–516.

Xypolias, P., Koukouvelas, I.K., 2001. Kinematic vorticity and strain rate patterns associated with ductile extrusion in the Chelmos Shear Zone (External Hellenides, Greece). Tectonophysics 338, 59–77.

Xypolias, P., Dörr, W., Zulauf, G., 2006. Late Carboniferous plutonism within the pre-Alpine basement of the External Hellenides (Kythira, Greece): evidence from U-Pb zircon dating. Journal of the Geological Society London 163, 539–547.

Yassaghi, A., James, P.R., Flottmann, T., 2000. Geometric and kinematic evolution of asymmetric ductile shear zones in thrust sheets, southern Adelaide Fold-Thrust Belt, South Australia. Journal of Structural Geology 22, 889–912.

Yonkee, A., 2005. Strain patterns within part of the Willard thrust sheet, Idaho-Utah-Wyoming thrust belt. Journal of Structural Geology 27, 1315–1343.

Zulauf, G., Kowalczyk, G., Krahl, J., Petschick, R., Schwanz, S., 2002. The tectonometamorphic evolution of high-pressure low-temperature metamorphic rocks of eastern Crete, Greece: constraints from microfabrics, strain, illite crystallinity and paleodifferential stress. Journal of Structural Geology 24, 1805–1828.